Impact of Planar Microcavity Effects on Light Extraction—Part II: Selected Exact Simulations and Role of Photon Recycling

H. Benisty, H. De Neve, and C. Weisbuch

***Abstract*— In this paper we use an exact calculation of dipole emission modifications in an arbitrary multilayer structure to obtain the extraction efficiency from realistic planar microcavities. Additional insights gained through this exact approach compared to the simplified one of Part I of this paper are first discussed in the case of a dielectric slab. We next optimize for the extraction purpose asymmetric cavities bounded by metal on one side and dielectric mirrors on the output side for any pair of material indices in a broad range (n = 1.4–4). The decrease of extraction when taking into account relative linewidths of the source of a few percent is shown to be moderate, allowing the large enhancements of monochromatic light to be maintained in many useful cases. The fractions of power emitted into guided modes, leaky modes, etc., are detailed. The beneficial role of possible photon recycling (reabsorption of emitted photons by the active layer) on extraction efficiency is evaluated using the fractions of power in guided and leaky modes. Extraction efficiencies in the 50% range are predicted for optimized, hybrid, planar metal–semiconductor structures for a wide range of active materials and wavelengths. We show that exact calculations justify the simple model used in Part I evaluating the extraction efficiency of a microcavity-based light-emitting diode as $1/m_c$ where m_c is the effective cavity order.**

***Index Terms*— Cavities, distributed feedback devices, Fabry–Perot resonators, light-emitting diodes, light sources, microcavities, semiconductor device modeling.**

I. Additional Insight From the Exact Approach

IN PART I [1], we used a scalar model and made a number of simplifying assumptions in order to clarify the main trends of light extraction from microcavities in high-index emitting materials. We showed why, through the number of competing Fabry–Perot (FP) modes, a small cavity order was essential to obtain sizable extraction enhancement. The main analytical results in this respect are the following: [1, eq. (8)] defines a microcavity regime with a "threshold" cavity order m_c for which a single mode is extracted as $m_c \leq 2n^2$. The limit extraction in this regime as $\eta = 1/m_c$ is given by [1, eq. (7)], and [1, eq. (15)] gives the modest top mirror reflectivity for which one obtains most of this extraction: $R_1 = 1 - m_c/n^2$. These basic equations are translated to distributed Bragg reflectors (DBR's) by [1, eqs. (23)–(26), (28)] while [1, eqs. (30), (31)] apply to the case of a different aperture requirement, e.g., for coupling to fibers.

The price paid for this simplicity was to drop polarization effects, to consider reflectivity as a constant independent of wavelength and angle, to use at best piecewise constant reflectivities to depict DBR stopbands, to take isotropic sources instead of electric dipoles, and to put aside antinode factors.

We turn here to rigorous calculations of more realistic structures. The large number of parameters of any actual microcavity emitter structure (many frequency-dependent complex indices and thicknesses, antireflection coating, natural spectrum versus injection level, etc., precludes exhaustive studies (for a discussion of these issues in no-cavity light-emitting diodes (LED's), see, e.g., [2], [3]). However, we found that by choosing a structure for which optimization still preserves some versatility of performances, we could define a useful starting point to carry on selected parametric studies that bring much additional insight over the analytical approach.

We briefly discuss in Section II-A a rigorous model based on the late 1970's work by Lukosz and others [4]–[6] that gives the output power radiated by electric dipoles of arbitrary orientations for each of the two polarizations s (TE) and p (TM) [7]. In Section II-B, we first apply this model to extraction of s-polarized (TE) light from a mere plane homogeneous slab of high index $n = 3$. In particular, we illustrate through this exact approach concepts relevant to the balance between power emitted in guided modes versus power in outside modes. We turn in Section II-C to general results (scaling issues) for a typical asymmetric microcavity configuration analogous to [8], [9] generalized by allowing for any pair of realistic material indices for the two materials taken to form the DBR mirrors and the cavity. In Section II-D, we first study how monochromatic extraction efficiency evolves upon detuning off the optimal wavelength. We next calculate extraction efficiency as a function of the source natural linewidth, which applies to the situation of many actual devices.

Section III is devoted to the welcome benefits of the photon recycling mechanism possibly existing in many devices [10]–[13]. This mechanism rests on reabsorption of light emitted by the active region, of interest for light emitted into modes other than outside modes (guided or leaky modes). The possibility of successive cycles of emission absorption increases the probability for energy to be eventually radiated outside, which means, in other words, increasing the device

Manuscript received November 6, 1997; revised May 18, 1998. This work was supported by ESPRIT Basic Research Project SMILES 8447.

H. Benisty and C. Weisbuch are with the Laboratoire de Physique de la Matière Condensée, UMR 7643 du CNRS, Ecole Polytechnique, 91128 Palaiseau cedex, France.

H. De Neve is with the Department of Information Technology, University of Gent-IMEC, B-9000 Gent, Belgium.

Publisher Item Identifier S 0018-9197(98)06232-0.

overall electrooptic conversion coefficient over the simple product of internal quantum efficiency by extraction efficiency [11], [13], [14]. It is a welcome effect in any emitter, provided internal quantum efficiency is sufficient to sustain as many emission-absorption cycles as needed. We show here that, due to their superior intrinsic extraction performance when compared to bare structures, microcavities feature a sizeable improvement with much less demand on internal efficiencies, namely not beyond currently existing levels in industrially grown materials. Section III-C finally focuses on results for specific existing and future LED material systems among III–V's [15]–[29] and II–VI's [30]–[33]. In many cases, extraction efficiencies of the order of 50% seems possible.

II. Exact Extraction from Realistic Microcavities Without Photon Recycling

A. Exact Emission Pattern and Power Calculations

We apply in this paper an exact model of dipole emission in a multilayer detailed elsewhere [7] to situations with realistic reflectors and sources. This model partly relies on a classical transfer-matrix description and gives results identical to other approaches [34]–[36] based, e.g., on dipole coupling to externally impinging modes. Its originality lies in the direct use into the transfer-matrix formalism of additive source terms for each in-plane Fourier component $k_{//}$ of electric field [4]–[6], even those corresponding to waves evanescent in the source layer. This circumvents the explicit description of dipoles near-field [37] and captures only the resulting far-field emission pattern. It also offers the opportunity to quantify emission in guided and leaky modes and environment-induced lifetime modifications.

We first depict the case of s-polarized emission of a horizontal dipole in a mere $n = 3$ slab, where we enlighten specific contributions of the exact approach and gain insight on guided mode behavior. This is a useful example where we purposely restrict to a specific dipole orientation and a single polarization. The reason is that further calculations which include all cavity parameters, polarizations, etc., do not lend themselves to this heuristic point of view. We next turn to the main purpose of this section, asymmetric DBR/cavity/metal structures akin to microcavity LED devices [8], [9], [36], where we explore scaling issues with the combined benefit from the approximate and exact aproach: for these asymmetric cavities, we examine how results from the (InGaAl)As testbed system [8], [9] may be extrapolated to any practical pair of DBR indices. We also detail the influence of natural linewidth. Results reported in this part are intended as guidelines. They are not meant to account for all details of real systems such as exact injection-dependent lineshape of LED's [8], optical constant dispersion, thermal effects, epoxy packaging, etc. [38], that are tasks of device implementation, although their influence may be approached using the concepts outlined in [1].

B. The $n = 3$ Slab

We start with a mere slab of index $n = 3$ and thickness d surrounded by vacuum and vary its optical thickness nd to scan

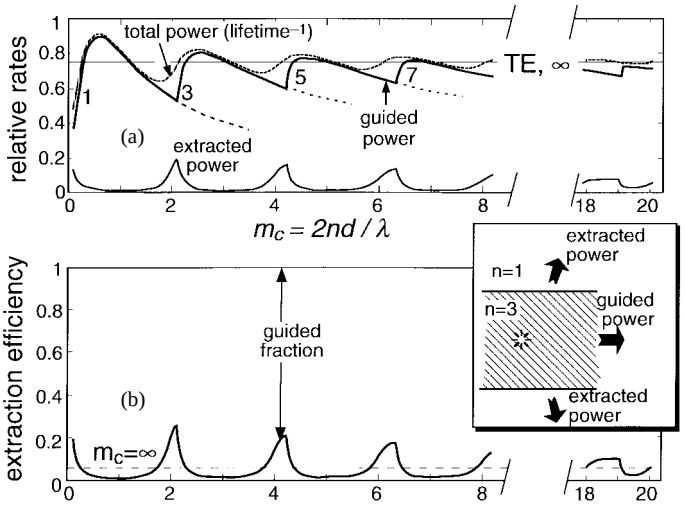

Fig. 1. (a) Power extracted and guided into s-waves (TE) from centered horizontal dipoles in an $n = 3$ slab depicted in the inset below as a function of its reduced optical thickness. Total power accounts for lifetime effects. (b) Extraction efficiency $\eta = P_o/(P_o + P_g)$.

through mode cutoffs and cavity orders [39]. In order to retain a heuristic viewpoint, we restrict ourselves to monochromatic s- polarized emission of a centered horizontal (h) dipole sheet (inset of Fig. 1) because: 1) its emission pattern is isotropic (see [7]); 2) Fresnel reflection coefficients gently increase from 25% to 100% from normal to grazing incidence, unlike p-polarized waves; and 3) (h) dipoles emit 75% of their power into s-waves. Since our exact approach makes use of normalized $(s + p)$ emission, total emission enhancement or inhibition (emitter lifetime modifications) applies here relative to $P_{\rm ref} = 0.75$, not unity. For simplicity, we call "power" the normalized power $P_{\rm tot}$ per dipole which may deviate here from 0.75 due to the effect of optical environment.

We calculated power extracted in all vacuum modes P_o as a function of reduced optical thickness $nd/\lambda(\approx 2m_c)$, as well as power in all guided modes P_g, using an *ad hoc* thin damping layer (see [7]). These powers are plotted in Fig. 1(a) for order up to the microcavity regime limit defined in [1] $m_c \sim 2n^2 = 18$. It appears that, as stated, total power per dipole $(P_o + P_g)$ is modulated, even in such a moderate cavity. The rigorous extraction coefficient $\eta = P_o/(P_o + P_g) = P_o/P_{\rm tot}$, which generally differs from $P_o/P_{\rm ref}$ by not more than 15% except for $nd/\lambda \ll 1$, is plotted on Fig. 1(b). Due to symmetry, only odd guided modes $m_c = 1, 3, 5, \cdots$ (those with even profile in our notation) couple to dipoles.

Striking increases in η or P_o arise each time a new FP mode appears at normal incidence. This increase starts before resonance, when the Airy peak tail begins entering the escape window. It continues as the peak fits well inside the escape window and the resonant outside angle becomes off-normal. Next, toward grazing outside incidence, it is more surprising that P_o "saturates" instead of decreasing as the Airy peak starts getting out of the escape window. But this is due to the increased s-reflectivities reaching 100% and allowing to infinitely sharpen the Airy peak into a vanishing angular window, a feature absent in [1].

Just after this situation, the FP mode turns to a new guided mode (cutoff condition) and guided power P_g abruptly swells

to the expense of outside power. Each such new guided mode then goes through a maximum coupled power. This behavior was pointed out a long time ago by Wittke for spontaneous emission coupled to the fundamental guided mode in double-heterostructure lasers [40], [20], [16]. This optimal dipole-guided mode coupling results from a minimal extent of field profile, hence a larger field amplitude per photon: the field profile just above cutoff has extended tails that first shrink as d keeps increasing, allowing the mode/slab overlap to increase toward unity and field amplitude at the source to grow. Beyond this situation, as d still increases, the width of the field profile just follows this increase and coupling reduces again, naturally making room for the next mode.

Note that extrema of P_o, P_g, and $P_o + P_g$ occur at different points of this cycle, following the balance of enhancement/inhibition of both categories of modes at a given optical thickness. The strong modulation of P_o and η at small orders dampens at higher orders. On the right of the figure is the microcavity regime limit: odd resonances occur no more in narrow conditions but through one-half of cavity orders. In between, even modes are resonant and both resonances would start to coalesce if even modes were coupled. The microcavity threshold for a centered source is apparently doubled here $(m_c \sim 4n^2)$ because the symmetry halves the relevant optical thickness.

Before turning to DBR-based cavities, let us give a hint of total emission in $(s+p)$ modes of the above (h) dipole: there is also a succession of p (TM) modes much like the s case, with one p mode intercalated between each s mode for such a simple cavity. Tails of p (TM) modes just above cutoff condition are far more extended than s (TE) ones due to the different field boundary condition. This results in a lower coupling to the fundamental p (TM) mode as pointed out by Ho *et al.* [41] for excitons.

The same authors also noted a quite dramatic reduction of the vertical (v) dipole emission in very thin layers (p-polarized of course). They suggested important consequences for extraction of isotropic dipoles: since extraction of vertical dipoles is almost zero in microcavities due to their $\sin^2\theta$ basic pattern, emission of vertical dipoles is a waste of power. Thus, inhibition of overall emission from vertical dipoles (larger lifetimes) is undoubtedly beneficial to extraction. Whether it can be achieved while enhancing (h) dipole emission will be discussed quantitatively below. Qualitatively and briefly, the large differences between (h) and (v) dipoles can be easily understood using image dipoles to capture the phase of reflected waves: when the dipole is located at an antinode, the field from the vertical dipole image is out-of-phase in the horizontal emission plane, whereas in the converse (h) dipole case, it is of course in-phase, especially in the vertical direction.

C. Asymmetric Cavities with DBR and Metal: The Monochromatic Optimum

We may now combine the physical understanding gained in [1] with the accurate predictive power of the complete calculation to explore the important issue of extraction from asymmetric microcavities with a DBR on one side and an absorbing metal on the other side. We recognized in [1] the potential of this configuration: low cavity order and compatibility of the DBR mirror with epitaxial growth of heterostructures. Such an investigation is all the more prompted by the recent success achieved in this field [8], [9], [13], [42]–[46], and the large impact envisioned for LED devices.

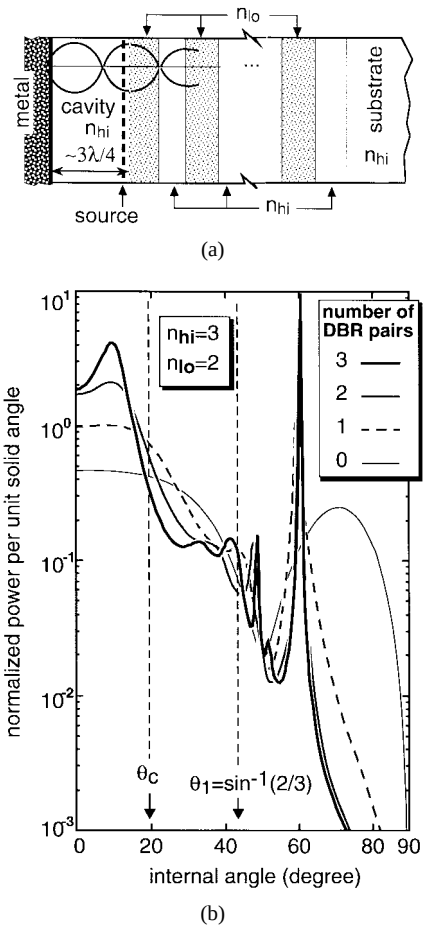

Fig. 2. (a) Typical asymmetric microcavity LED structure with the schematic extracted mode profile. (b) Emitted power angular pattern (both polarizations) for an horizontal dipole in the case of $n_{\rm hi} = 3, n_{\rm lo} = 2$ and $n_{\rm met} = 0.3 + 5i$ and for $p = 0$, 1, 2, and 3 DBR layer pairs. Total internal reflection angles for outside index and $n_{\rm lo}$ are indicated.

To reduce the huge number of parameters of such a situation, we assume that the source is not distributed, but unique, located at the second antinode of a $3\lambda_B/4$ cavity, just aside from the DBR mirror (see Fig. 2) with normal incidence nominal wavelength λ_B. Such a short bare cavity gives of course an upper estimate for extraction from larger ones. As for distributed sources, the extraction is essentially convolved by the mode profile, or equivalently by the position-dependent antinode factor ζ, essentially a standing wave varying like $\sin^2(2kz)$. Extraction is thus at worst halved when sources are evenly distributed across one or many half-wavelengths [4], [34], [36], [47]. Cavity and substrate share the DBR high index medium $n_{\rm hi}$. We define as extracted all the power emitted in the substrate below critical angle with air $(n_{\rm out} = 1)$, neglecting substrate absorption and assuming a standard antireflection coating at the substrate–air interface.

For extraction in epoxy ($n_{\rm out} \approx 1.5$) [2], [38], indices of all dielectrics have to be scaled accordingly. However, the frequent use in applications of the epoxy dome as a lens to shape the LED beam is better achieved with a divergence of $\sim$45° off-axis in epoxy. Then, from Snell's law, since $1.5 \times \sin(45°) \sim 1$, requiring 45° maximum incidence in epoxy amounts to require extraction in vacuum. Our essential MCLED parameters are: 1) the cavity index $n_{\rm hi}$; 2) the DBR low index $n_{\rm lo}$; and 3) the lossy metal complex index $n_{\rm met}$. Losses obviously limit extraction below the mode-counting prediction $\eta = 1/m_c$ [1]. It turns out that for typical indices of metals with good reflectivities such as gold and alloys in the visible and near-infrared [48], the optimal extraction for a perfectly monochromatic source corresponds to a moderate degree of resonance, that is a reflectivity not far from $R_1^{\rm crit}$. This is close to the boundary between regions A and D of [1, Fig. 8]. This means that for typical spectral width $S = \Delta\lambda/\lambda$ of a few percent (not above line X in [1, Fig. 8]), the monochromatic configuration is still very close to the optimum. Here we take $n_{\rm met} = 0.3 + 5i$, a realistic value for noble metal-based contacts.

We actually optimize horizontal dipole monochromatic extraction η_h fully taking lifetime effects into account ($\eta_h = P_{\rm out}/P_{\rm tot}$ for horizontal dipoles), just as in the previous subsection: for a given structure we scan (reduced) wavelength through resonance and determine extraction at the best wavelength. Optimization of the number of Bragg pair $p^{\rm opt}$ follows, resulting in a $(\lambda^{\rm opt}, p^{\rm opt})$ couple. Typical successive angular emission patterns at the best wavelength and increasing p from 1 to $p^{\rm opt}$ are presented in Fig. 2(b) illustrating the FP resonance build-up in the case $n_{\rm hi} = 3$ and $n_{\rm lo} = 2$. Here, beyond $p^{\rm opt} = 3$ pairs only, metal losses become detrimental.

We present in Fig. 3 two contour maps for a useful part of the $(n_{\rm lo}, n_{\rm hi})$ plane with contours of data found when optimizing extraction of the structure of Fig. 2(a). In map (a) are delineated regions where the optimal number of layer pairs is $p^{\rm opt} = 1, 2, 3, \cdots$. Solid contours show the optimized monochromatic extractions η_h for the sole (h) dipole. These contour maps are to be compared to [1, Fig. 11] giving the results of the analytical approach for the same system. Let us first comment the small Δn region, close to the diagonal: in this region, $p^{\rm opt}$ is large and essentially scales like $n/\Delta n$. This region displays the steepest increase in extraction when starting from $\Delta n = 0$ at fixed $n_{\rm hi}$. The crude approximations of cavity order $m_c \approx n/2\Delta n$, neglecting $m_o = 3/2$, and the simplified rule $\eta = 1/m_c$ imply that extraction grows linearly with Δn in this region. It is thus seen that Fig. 3 reproduces well the trends found in [1] in the same region. This confirms our claim that the analytical approach is relevant in the relatively small Δn limit ($\Delta n < 1$), and is useful to establish the scaling laws of microcavity LED's. For very small index steps however, namely when $n\Delta n < 1/4$, one leaves the single-extracted-mode microcavity regime toward a "meso-cavity regime" evoked in [1, Appendix C]. Also, it is clearly interesting in this case to consider a short DBR assisted by the Fresnel reflection at the DBR–air (epoxy) interface (see [1, Section II-F]).

Turning to regions of larger index steps, a plateau in extraction is reached typically for index steps ranging from

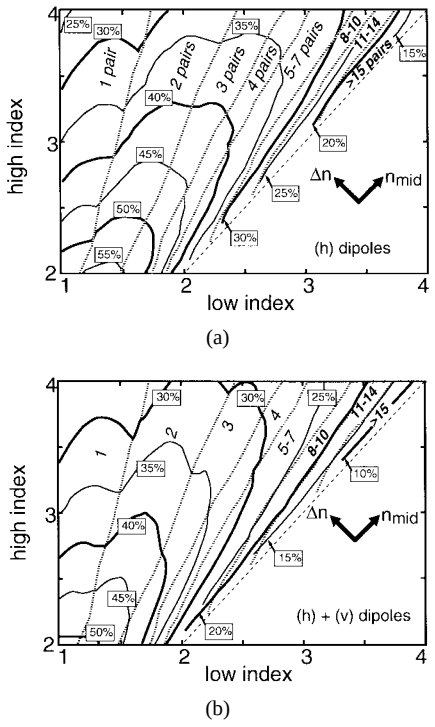

Fig. 3. (a) Solid lines: contours of equal optimized extraction efficiency η_h from a monochromatic horizontal (h) dipole in the structure of Fig. 2(a) in the $(n_{\rm lo}, n_{\rm hi})$ plane; dotted lines bound regions of given optimal number of DBR layer pairs $p^{\rm opt} = 1$ pair, 2 pairs, 3 pairs, etc. (b) Same for an isotropic dipole. Lifetimes are taken into account. Note that in in the $(n_{\rm lo}, n_{\rm hi})$ plane, axis for average index $(n_{\rm lo} + n_{\rm hi})/2$ and index difference $\Delta n = (n_{\rm hi} - n_{\rm lo})$ are at 45°.

$\Delta n = 1$–1.5. In this region, the number of pair $p^{\rm opt}$ falls from 5–7 to 2. Then, due to the use of simple pairs, one clearly misses the optimal reflectivity especially at each of the $p^{\rm opt}$ boundaries where reflectivity is too high on one side and too low on the other side. The trend toward larger extraction at larger index contrasts not only saturates in the region $n_{\rm lo} = 2$, but becomes eventually inverted when the low index tends toward the outside one, $n_{\rm lo} = 1$. This is contrary to the prediction of [1] where it was argued that a decrease in m_c, subsequent to a larger Δn, translates into a larger extraction at given mirror losses. Reasons for this discrepancy are complex. We calculated that even in the absence of losses, extraction saturates for these large contrasts but that the decrease was apparent as soon as very weak losses were present. Analysis of these results showed that complex polarization effects arise when $n_{\rm lo} \to 1$. In particular, Brewster angles of TM modes for the DBR low-index medium and the outside medium become identical. It is thus difficult to build a TM resonance at the desired oblique outside angles. Instead, TM resonance and extraction are favored toward normal incidence whereas TE extraction is best at grazing outside incidence (cf. the slab case), so that at no wavelength can both extractions be simultaneously favored. The value of $\mathrm{Im}(n_{\rm met})$ also plays a role since it controls the fraction of field profile penetrating into the metal layer when the mode is squeezed into a smaller effective cavity toward $n_{\rm lo} = 1$. The full understanding of these effects is, however, still unsatisfactory.

As for an isotropic emitter instead of a horizontal (h) dipole, the map of Fig. 3(b) parallels that of Fig. 3(a), and also

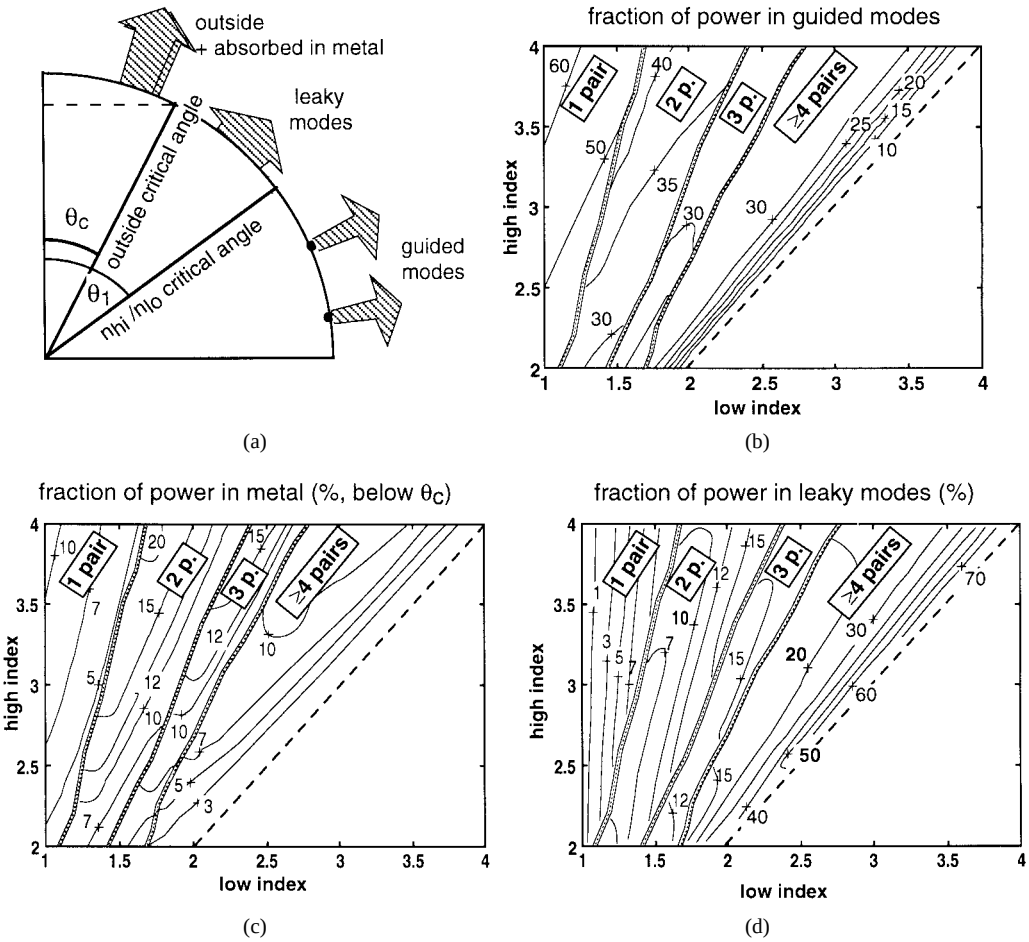

Fig. 4. (a) Sketch of the angular distribution of the various modes. (b)–(d) Smoothed contours in the $(n_{\rm hi}, n_{\rm lo})$ plane of the fractions of emitted power: (b) in the metal $(n = 0.3 + 5i)$, (c) in guided modes, and (d) in leaky modes; the regions of given pair number $p^{\rm opt} = 1$, 2, 3, and $p^{\rm opt} \geq 4$ are outlined because they correspond to abrupt variations of these fractions.

takes lifetime effects of the (h) and (v) dipoles into account. Trends are as follows: extraction from the sole vertical dipole is generally negligible due to its underlying $\sin^2\theta$ emission pattern. For small Δn, lifetimes effects are weak, so that the intuitive average, $\eta_{\rm iso} = (2/3)\eta_h$ with obvious notations, holds.

But, for $\Delta n \sim 1$, and still more above, the (h) emission rate (inverse lifetime) increases whereas the (v) rate vanishes. In these regions, $\eta_{\rm iso}$ thus recovers a value close to η_h, since emission of the vertical dipole tends to become a forbidden channel. The peculiar choice of the source location, close to the DBR, and the small bare cavity make this trend quite strong here.

Light not extracted goes into three categories: guided modes, leaky modes and metal absorption, as sketched in Fig. 4(a). This latter takes place at angles of the escape cone, fed by the resonant outside mode bouncing inside the cavity. We map in Fig. 4(b)–(d) the fractions of total emitted power $P_{\rm tot}$ in these three categories at the optimum situation of Fig. 3(a), taking lifetime effects into account $(P_{\rm tot} \neq 1)$, as explained for, e.g., extracted and guided power in the slab case, but with both polarizations here. This is still a monochromatic case and (h) dipole. In these three maps, abrupt variations stem from the discrete $p^{\rm opt}$ values of optimized structures under consideration. Regions where $p^{\rm opt} = 1$, 2, 3, and ≥ 4 are delineated for this reason.

Trends for the guided mode fraction $f_g = P_g/P_{\rm tot}$ are rather different from the naive expectation drawn from the solid angle subtended by the cone beyond $\theta_{\rm lo}$ where the DBR causes total internal reflection. Only the small Δn region (along the dashed diagonal) displays the expected rise in f_g, varying like $(\Delta n/n)^{1/2}$. But in a very wide region, f_g is around 30%, reaching 50% only close to $n_{\rm lo} \approx 1$.

The fraction f_{lk} emitted in leaky modes displays complementary variations and rapidly decreases when Δn increases, as predicted in [1, Appendix C]. It also exhibits a steady behavior in the intermediate regions of Δn, where it typically amounts to 15%–25% of the emitted power. But there is no room for these modes when $n_{\rm lo} \to n_{\rm out} = 1$ in our definition since their angular range is squeezed between ranges of guided and outside modes in this limit.

Finally, the fraction f_m of emitted power absorbed into the metal (here below θ_c) is seen to vary from a few percent to ~15%. The (largest) normal incidence reflection loss is typically 10% here $(n_{\rm met} = 0.3 + 5i)$ but concerns 20%–40% of emitted light (not guided, and on one side). The optimization leads to avoiding the large losses that would result from too strong reflectors and too many cavity round-trips: the f_m

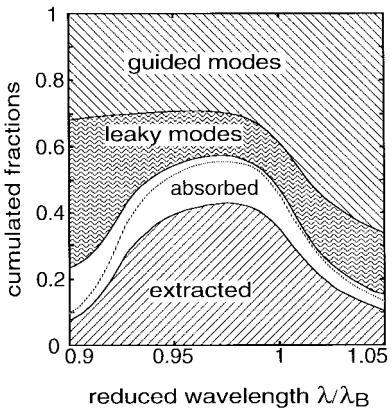

Fig. 5. Cumulated fractions as a function of wavelength around resonance of the power in the various channels: extracted, absorbed in the metal, in leaky modes, and in guided modes as indicated. The dashed line in the absorbed part separates the absorption occuring below and above the vacuum critical angle.

values clearly decrease across the boundaries of different p^{opt} regions.

D. Asymmetric Cavities with DBR and Metal: Spectral Trends

In any resonance problem, the two main parameters are the resonance position and its width. As for the resonance position, a first "spectral" result of the optimization procedure is the detuning between the Bragg central wavelength λ_B and the optimized wavelength for extraction, λ_{opt}: we start with the cavity resonant at λ_B at normal incidence and find a negatively detuned optimal extraction wavelength $\lambda_{\mathrm{opt}} < \lambda_B$. The results correspond to the simple trend of [1, eq. (10)], i.e., a resonance in the middle of the escape window ($\lambda_{\mathrm{opt}}/\lambda_B \sim 1\text{–}1/4n^2$), strongly shifted only for small cavity indices.

The most interesting aspect for the extraction issue is resonance linewidth. A typical plot of superposed fractions η, f_m, f_{lk}, f_g as a function of reduced wavelength λ/λ_B is shown in Fig. 5 for a cavity with $n_{\mathrm{hi}} = 3$ and $n_{\mathrm{lo}} = 2$. The extraction resonance is clearly visible. The trends of leaky modes to increase at short wavelengths was explained in [1, Appendix C] as due to the resonant mode angle evolving beyond critical angle θ_c and spanning through leaky mode angles. As for guided modes, we have qualitatively the same phenomenon due to a new mode as for the simple slab: at $\lambda = 1.05\lambda_B$, the resonant extracting mode is forbidden (below its cutoff). Toward shorter wavelengths, the cutoff of this mode is crossed ($\lambda \approx \lambda_B$) and the new resonant mode imposes a different power distribution favoring extraction to the expense of guided modes. At wavelengths around $\lambda \approx 0.9\lambda_B$, the power in this new mode is directed toward increasing angles and spans the swelling leaky modes. For still shorter wavelengths, $\lambda \sim 0.8\lambda_B$, guided modes tend back to their level at $\lambda = 1.05\lambda_B$.

Cavities optimized for monochromatic extraction may nevertheless successfully extract a sizable range around this optimized wavelength. In Fig. 6, we used a simple model to calculate the wavelength-integrated extraction of sources as a function of their natural own spectral width S_{source} in the case of optimized cavities with an emitting medium index $n_{\mathrm{hi}} = 3$ and various illustrative DBR low indices n_{lo} from 1 to 2.8,

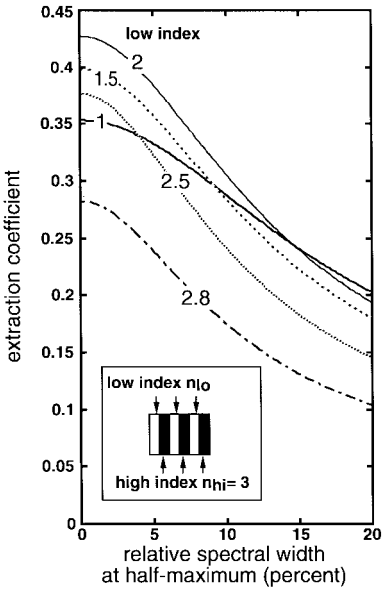

Fig. 6. Wavelength-integrated extraction from a source of Gaussian natural profile as a function of its relative spectral width at half-maximum for a system with a given high index $n_{\mathrm{hi}} = 3$ and the indicated low indices $n_{\mathrm{lo}} = 2.8$, 2.5, 2, 1.5, 1. The respective optimized number of layer pairs used in each case are 10, 6, 3, 2, 1.

this latter at the edge of the microcavity regime. We assumed a Gaussian spectral profile for the source as well as for the cavity extraction versus wavelength and refer to the width at half-maximum. It is seen that for the wavelength-integrated, half of the maximum monochromatic extraction is preserved up to a natural spectral width largely in excess of 10% in all cases, about ~15% for the low indices n_{lo} between 1.5 and 2.5, and about 20% for $n_{\mathrm{lo}} = 1$, which appears as a good solution for emitters with very large spectral widths. Let us notice, however, that the limiting factor is the threshold relative width $S_{\mathrm{esc}} = 1/2n^2$ found in [1, Appendix B]. Here, this threshold width of 5.6% defines the shoulder position of the five curves of Fig. 6. The use of epoxy instead of air as the output medium raises S_{esc} to the much more comfortable value of 12.5%. This leaves the possibility to benefit from microcavities also for long-wavelength strongly pumped light-emitting diodes where S may reach 15% (see Section IV).

To give a general map of the data of Fig. 6 is, however, not quite meaningful because it relies on the arbitrary choice of a source profile, Gaussian here. One may define with more generality a "relative wavelength shift tolerance" $S = \Delta\lambda/\lambda$ rather than a linewidth. It applies to the case of a relatively narrow source whose central wavelength varies due to temperature, for example, or other physical effects. We define this quantity as the range over which monochromatic extraction is maintained over 50% of the optimal (monochromatic) extraction, as suggested by the inset of Fig. 7, in which a contour map of these S values is given in the same $(n_{\mathrm{lo}}, n_{\mathrm{hi}})$ plane as above. Of course, since we do not consider here wavelength-integrated quantities, this width S is quite narrower than the width of Fig. 6 above, typically by a factor 0.7. It varies from $S = 4\%\text{–}20\%$ across the studied region. Results follow again the trends of Section II, with a spectral tolerance varying like $S_{\mathrm{esc}} = 1/2n^2$, decreasing at large

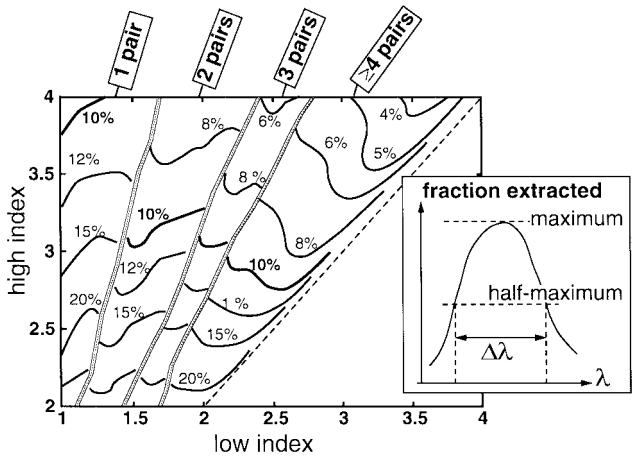

Fig. 7. Smoothed contours in the $(n_{\rm lo}, n_{\rm hi})$ plane showing the relative wavelength shift tolerance $\Delta\lambda/\lambda$ for which the extraction is maintained to over 50% of its peak value (scheme of the inset). Again, regions where $p^{\rm opt} =$ 1, 2, 3, etc., are outlined.

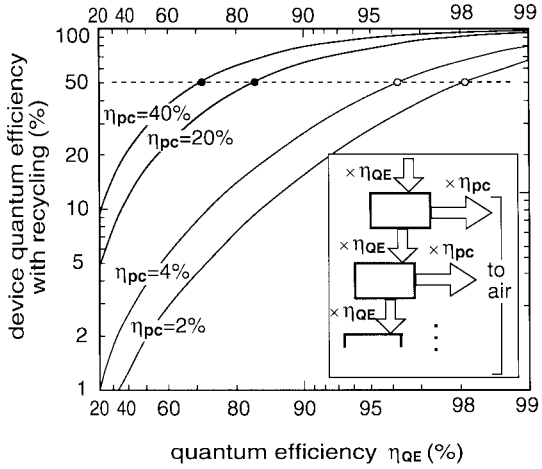

Fig. 8. Extraction efficiency as a function of the internal efficiency $\eta_{\rm QE}$ in an ideal case of recycling of all nonextracted light (scheme of the inset) on a log–log scale for different values of the extraction per cycle $\eta = \eta_{pc}$: the values 2% and 4% are representative of a standard device whereas 20% and 40% are for a microcavity emitter.

indices. Spectral tolerance is also rather broader for large index contrast $\Delta n \geq 1$, due to the better phase behavior of the DBR mirror, as in Fig. 6.

Details of emission diagrams, study of other metal indices, optimization with spectral width, aperture, polarization constraints, etc., will be discussed elsewhere. In the next section, we deal with the photon recycling phenomena which mainly concerns guided modes and leaky modes.

III. Enhancement from Photon Recycling and Extraction for Some Real Semiconductor Systems

A. Interest of Photon Recycling with Microcavity-Based Sources

It was recently demonstrated that in a very high-quality semiconductor, the mechanism of photon recycling could lead to a dramatic overall extraction efficiency (72%) in spite of the modest ~2% bare extraction efficiency [14]. In this mechanism, emitted light undergoes as many reabsorption and reemission cycles as necessary in the active layer, of the order of fifty cycles in the work mentioned [14] where the photon randomly samples momentum phase space until a favorable angle is found. It is, however, difficult to practically design an electrically pumped device based on this extreme example, which requires material with an internal quantum efficiency (radiative recombination probability) over 99.5% due to the poor escape probability per cycle. Sustaining so many cycles of reabsorption and reemission translates into a demand not only for a large internal radiative recombination quantum efficiency of the active layer, but also for negligible losses at metallic interfaces (removed beneath a silica optical layer in [14]), for a device large enough to accomodate the lateral spread intrinsic to the "radiative diffusion" process, etc., notwithstanding a low-speed penalty.

By strongly enhancing the escape probability per cycle (the nominal extraction calculated above, which will be termed here η_{pc}), microcavities greatly relieve all these demands and lead to far more practical device designs where the beneficial mechanism of recycling may push the overall extraction in the 50% range. To make this point more quantitative, we plotted in Fig. 8 results of the simplest model one can devise to evaluate how effective are the larger extractions per cycle attained with microcavities in relieving the demand on internal quantum efficiency. In this model, as pictured in the inset, a fraction denoted $\eta^{\rm QE}$ of injected carriers does undergo radiative recombination (rectangle), with the remainder fraction $1 - \eta^{\rm QE}$ undergoing nonradiative processes. In this simplified model, photons can only escape (with probability $\eta = \eta_{pc}$) or induce new carriers by reabsorption (with probability $1 - \eta_{pc}$), which then undergo similar events, no photon being truly lost. It is trivial to sum the series and find that the effective extraction, i.e., the fraction $\eta_{\rm eff}$ of injected carriers converted into outside photons simply reads

$$\eta_{\rm eff} = \frac{\eta_{pc}\eta^{\rm QE}}{1-(1-\eta_{pc})\eta^{\rm QE}}. \tag{1}$$

This quantity is plotted in Fig. 8 on a log–log scale as a function of $\eta^{\rm QE}$ for four values of η_{pc}: smaller ones, $\eta_{pc} = 2\%$ and 4%, are typical of "bare" systems without microcavities, whereas larger ones, $\eta_{pc} = 20\%$ and 40%, are typical of extraction-optimized microcavity sources. It clearly appears that for the two smaller cases (open dots), reaching, e.g., $\eta_{\rm eff} =$ 50% requires very large quantum efficiencies, here over 98% and 96%. The demand diminishes to a far more reasonable level for microcavity-type emitters, where it amounts to $\eta^{\rm QE} =$ 61% and 83% (solid dots), much closer to typical quantum efficiencies of industrially produced semiconductor layers (say, 80%–90% [49]).

B. Photon Recycling in Microcavity-Based Systems

Recycling is to be considered for both guided and leaky modes. Both modes experience some losses in the very emitting layer, a loss mechanism that was not taken into account above chiefly because it leads to recycling.

Besides, for guided modes, the absorption coefficient is large only for thick unpumped active layer. It is relatively low in the converse and common situation of thin or strongly pumped layers near transparency: for an active layer consisting of a few quantum wells, the absorption coefficient α becomes essentially $\Gamma\alpha$ where Γ is the mode confinement factor [16], [20] and may be a few percent per quantum well. In this case, losses "per round trip" are very weak and could be safely neglected in the above calculation of η_{pc}.

Recycling can, however, be maintained at a large level for guided modes even under such conditions if no other mechanisms such as metal losses compete to dissipate the optical power of guided modes. A lengthscale of the order of tens of microns is typical of guided mode absorption length, which justifies that they were neglected when studying the one-step extraction mechanism.

In principle, it is possible to recycle as well some part of leaky modes. But the picture for these modes is not so clear-cut: for a metal bounded structure, leaky modes have a larger interaction with the metal layer and are more prone to be dissipated in the metal than guided modes. For dielectric DBR mirrors on both sides, these modes could be irreversibly lost in the semiconductor substrate unless the cavity stack is lift-off and deposited on a low-index (silica) substrate, which allows total reflexion of most of the leaky modes back into the cavity. Therefore, we can only rely on the single-pass reabsorption of leaky modes as a worst-case method of recycling.

If we want to compare this situation with that without recycling, we can, to avoid too many details, limit ourselves to the calculation of the effective extraction η_{eff} obtained for 100% internal quantum efficiency and for a known coefficient for recycling of guided modes and leaky modes: assuming that fractions A_{guid} and A_{leak} of the power emitted into guided modes and leaky modes, respectively, are reabsorbed in the active layer, it is straightforward to modify the above formula by noting that the reinjected light is a fraction $f_g A_{\text{guid}} + f_{lk} A_{\text{leak}}$ of total power, where we recall that f_g and f_{lk} are the fractions of power emitted in the corresponding modes. The sum of the series for η_{eff} then reads

$$\eta_{\text{eff}} = \frac{\eta_{pc}}{1 - f_g A_{\text{guid}} - f_{lk} A_{\text{leak}}}. \tag{2}$$

In Fig. 9, we inject for η_{pc} the extraction of optimized asymmetric LED structures of Section II-C (monochromatic case, horizontal dipole) to plot contour maps of the resulting effective extraction η_{eff} in the usual $(n_{\text{lo}}, n_{\text{hi}})$ plane for two illustrative situations, chosen as monochromatic for simplicity: in Fig. 9(a), a very favorable recycling is assumed, where $A_{\text{guid}} = 0.8$ and $A_{\text{leak}} = 0.3$, i.e., most of the guided modes are recycled, and in Fig. 9(b) a more pessimistic case, $A_{\text{guid}} = 0.5$ and $A_{\text{leak}} = 0.0$ (no recycling of leaky modes). Again, this yields an upper estimate since factors such as radiative quantum efficiency, excitation of vertical dipoles, and finite linewidth are neglected.

The results show that even in the pessimistic assumption of Fig. 9(b), moderate index steps are sufficient to reach effective extractions close to 40%, and larger steps ensure 50% around $n_{\text{hi}} = 3$. Of course, the optimistic assumption of Fig. 9(a)

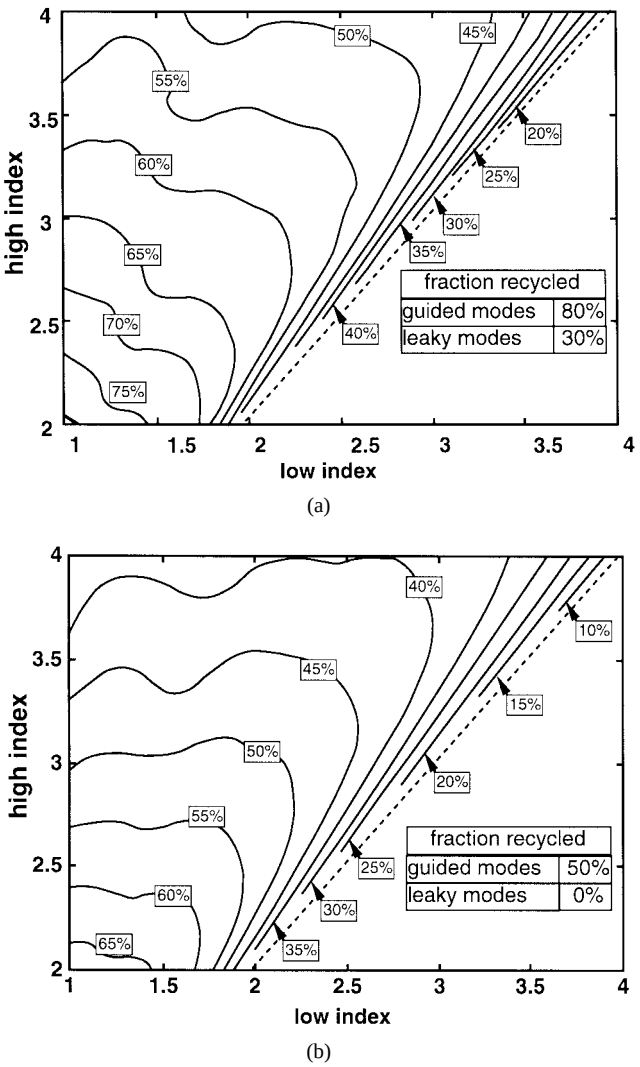

Fig. 9. Smoothed contours of extraction efficiency with recycling. (a) Eighty percent of guided modes and thirty percent of leaky modes are recycled. (b) Only 50% of guided modes are recycled.

brings up impressive performances, often over 60% extraction. If such an efficient recycling can indeed be realized (and there is no major physical reason why it could not), it is likely that the overall electron–photon efficiency of the device would still remain close to 50% even with the adverse factors mentioned above. Finally, the device response time is certainly slowed down by the recycling phenomenon, typically by the same factor as in (2). We may readily notice that this penalty is not more than a factor of two for microcavities, which is eventually much less than it would be starting from a low-extraction device because less recycling is intrinsically needed. Because high-speed LED's also raise the linewidth and injection-level issues, the rest of this discussion is in Section III-C.

C. Results for Existing LED Materials Systems and Discussion

In this section, we select a few among the main opto-electronic semiconductors that can be used for LED's and discuss what extraction performances can be expected at room temperature (RT) in view of their indices, linewidth, etc. A first broad classification concerns the natural linewidth. The

TABLE I
SOME EXISTING SEMICONDUCTOR SYSTEMS FOR LED'S, THEIR BANDAGAP ENERGIES (WAVELENGTHS), INDICES OF EMITTER, INDEX DIFFERENCE OF DBR'S, AND RELATIVE SPECTRAL WIDTH AT ROOM TEMPERATURE, SOME TIMES FOR VARIOUS SUB-CASES, WITH THE REFERENCE FOR SPECTRAL DATA

System	Short name	Direct bandgap range (eV)	Emitter index	Index difference Δn	Relative natural spectral width S=Δλ/λ	Reference for S
(Ga,Al,In)N	III-N	2.6 – 3.3	2.8±0.1	0.4	4 % at 450 nm (>3% at 380 nm, 7% at 515 nm)	[24]
(Ga,Al,In)P	III-P	2.0 – 2.2	3.2±0.1	0.3	~ 3 %	[28]
(Ga,Al,In)As	III-As	1.2 – 1.8	3.5±0.2	0.5	~ 4.5 % at 850 nm (>3% at 660nm)	[15,19]
(Ga,Al,In)As/Alox	III-As Al2O3	1.2 – 1.8	3.5±0.2	1.8	~ 4.5 % at 850 nm	see above
1.3 μm ternaries on InP	1.3 μm	0.85 – 1.05.	3.4	0.19	~ 8 %	[53]
1.55 μm InGaAsP quaternaries on InP	1.55 μm	0.80	3.35	0.26	~ 9 %	extrapolated from above case.
(Zn,Cd,Mg)(S,Se) 500 nm	500 nm II-VI (ZnSe)	2.4–2.6	2.8	0.15	~ 2.5 %	S=2.5 kT/E_g is used
HgCdTe mid infrared alloys	4 μm MCT	0.40	2.8	0.11	~ 30 %	[50]

naive approximation based on a mere Boltzmann distribution of injected carriers in ideal bands, $S \sim 2kT/E_g$, is often too crude for real structures that feature rather broader linewidth. However, it is clear that long-wavelength systems (1.3 and 1.55 μm and beyond) typically feature linewidths close to 10% which exceed by as much as a factor of two the threshold relative width $S_{\text{esc}} = 1/2n^2$ found in [1, Appendix B]. Then extraction roughly falls below the monochromatic optimal value by the same factor S/S_{esc} (see the example of Fig. 6, where S_{esc} is 5.5%).

Table II summarizes typical indices, index steps (see references below), bandgap energy, and natural linewidth of electroluminescence at RT of a number of III–V and II–VI semiconductor systems ranging from the ultraviolet-blue wavelength range to the midinfrared range. Let us discuss briefly linewidth issues in each system.

Starting with the III–V nitrides [21]–[26], we find that the linewidth is good (2.6%) for the UV electroluminescence (380 nm), but appreciably degrades for blue emission (~4% at 450 nm), (our choice for this system) and still more for green emission (7% at 510 nm). The next III–V system is AlInGaP, for which very efficient transparent-substrate LED's already exist, called "high-brightness LED's," although light is extracted by the sides of the chip [28], [9]. There, electroluminescence is narrowest (2%) at 550 nm thanks to the absence of doping but degrades to 3% at 625 nm, for the most luminous red LED's, for which doping is needed. The most classical III–V system is (GaAl)As, [15]–[18], [20]. Addition of indium in the wells allows up to 1-μm wavelengths. We retained the parameters of the important near-infrared range for free-space applications (850–900 nm typically, where cheap Si photodiodes are best) for which the large index contrast of AlAs–GaAs $(\Delta n = 0.5)$ is retained. The linewidth S is typically 4%–5%, close to the limit S_{esc} in air. The case of 670-nm LED's based on AlGaAs, with a linewidth $S = 3\%$ [19], makes use of Al-rich $Al_xGa_{1-x}As$ ternaries. These suffer from a lower index contrast $(\Delta n = 0.3)$ and can therefore be treated for microcavity prospects as the AlInGaP materials in a first approach.

The long-wavelength phosphide-based quaternaries grown on InP (1.3 and 1.55 μm) [16]–[18], of importance for fiber-based and eye-safe applications, offer less obvious prospects, because they combine low refractive index contrast ($\Delta n =$ 0.2–0.25) and linewidths of 80–120 nm: these latter broaden with increasing injection level, which is often used to improve the LED's speed parameters, as discussed below.

ZnSe-based II–VI's [30]–[33] have been included as potential green sources, although the recent successes of nitrides rather jeopardize them. It is not clear whether their linewidth at 500 nm could be an advantage in this competition. As far as II–VI are concerned, we also included HgCdTe-based far-infrared emitters (~4 μm) [50]. In the proposed systems, the index difference comes from the need of lattice-matched growth within 1% or so.

Fig. 10(a) gives in the same order their monochromatic extraction for isotropic dipole, [cf. maps of Fig. 3(b)] compared to the far mirror no-loss case $(\eta \approx 1/2n^2)$. Fig. 10(b) gives again this no-cavity reference but takes into account natural linewidth as in Fig. 6, which translates into lower extraction than the monochromatic optimum. In the two left bars of each system, an isotropic dipole was assumed.

In the two right bars, a horizontal (h) dipole, yielding intrinsically more extraction, was chosen. It is predominant in the electron–heavy-hole recombination of many III–V quantum-well materials [9], [16], [51]. The two estimates are: 1) without recycling and 2) with 70% recycling of guided modes $(A_{\text{leak}} = 0; A_{\text{guid}} = 0.7)$, an assumption intermediate between the estimates (a) and (b) of Fig. 9.

The results of Fig. 10 are intended as guidelines since the particular cavity size, metal losses, etc., do not necessarily correspond tightly to realistic configurations due to technological factors others than the considered lattice-matching issue. But the choice of, e.g., losses and cavity size is an intermediate one, useful as a starting point. Namely, not much can be gained in

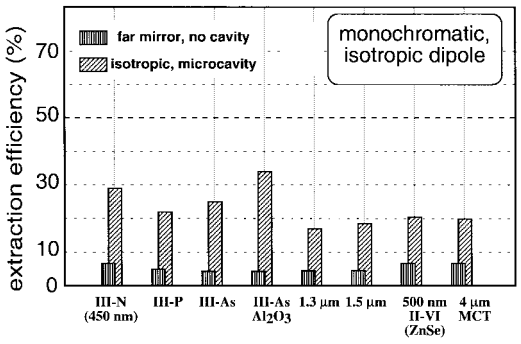

(a)

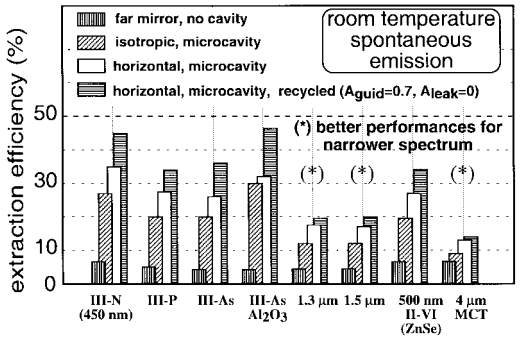

(b)

Fig. 10. Compared extraction performances. (a) Comparison of extraction for the various systems of Table II with a cavity and with just a far mirror (factor of two over bare extraction) at the best wavelength and for isotropic dipole. (b) Extraction taking into account the spectral width at room temperature for, respectively, isotropic dipole, the horizontal dipole, and the horizontal dipole with recycling of 70% of guided modes only. The far-mirror extraction has been kept for reference. For the long-wavelength systems labeled $(*)$, narrow spectra are often desired, which, compared to the no-cavity case, would lead to better performances.

terms of cavity size. As for metal losses, they typically amount to 10% of emitted power. Although metallic reflection tends to improve toward the infrared, technological requirements on contacts may lead to the use of quite poor metallic systems, with large absorption as well as some roughness. This would lead to consider a DBR, or a hybrid DBR–metal stack as the back mirror. At the other end of the spectrum, at blue wavelengths, this may also be the case due to the large losses of any metal in this case.

Also, packaging in epoxy would give increased figures. In particular, it raises the threshold linewidth $S_{\rm esc}$ which can be well extracted from the range 4%–7% to the range 9%–14% which is crucial to long-wavelength emitting diodes ($\lambda = 1.3$ μm and beyond), all the more if they are strongly pumped. This has to be studied separately, since fiber-coupling is often an additional issue in these systems. In general, an application-wise evaluation depends on the chosen photometric figure of merit, a choice which cannot be easily generalized. Hence, we chose extraction to air (and to a lesser extent brightness, see [1, Section II-E]) as a testbed of crucial figures of merits to illustrate the potential of microcavities in improving light emitters.

It clearly appears in Fig. 10 that the index difference of the DBR side is the crucial parameter in determining performance improvements. The long-wavelength systems labeled with $(*)$ also suffer in terms of total extraction from the fundamental limits of planar microcavity resonators as discussed in [1, Section II-E] and Section II-D here: for a relative spectral width exceeding $1/2n^2$, only a part of the spectrum is resonantly extracted, leading to a decreased wavelength-integrated extraction performance. The cavity's own spectral width, Fig. 7, is a basic measure of this phenomenon, a more exact result being the full spectral profile pictured in Fig. 5. We insisted above on the impact of epoxy packaging in relieving this index-limited cavity linewidth. But the natural spectral narrowing of extracted light from microcavity LED's (RCLED's [36], [52]–[54]) is indeed welcome for the specific needs of optical fiber links, where it increases the transmission range by reducing the limiting chromatic dispersion [36], [55]. Thus, for these applications, one should at least consider the monochromatic extraction η, which easily reaches the 20%–30% range, making electrooptic conversion coefficients closer to those of lasers. The relevant figure of merit for this application is rather the ratio of extraction to relative spectral width, i.e., $\eta(\lambda/\Delta\lambda)$. It is far more improved than integrated extraction due to the strong wavelength selectivity achieved by an ideal cavity observed within the typical numerical aperture of a fiber $(\sin\theta \approx 0.2)$ which reads $\Delta\lambda/\lambda \sim \sin^2\theta/2n^2$, and is typically a few tenths of a percent for an ideal resonator.

A last discussion is required to take into account speed requirements. First, it is clear that recycling slows down the device response by an amount equal to the gain in the extraction of (2), not a large factor in general. This means that in spite of an apparent lower cutoff frequency, the absolute differential efficiency $\Delta P/\Delta I$ at frequency ω above the cutoff frequency (single response time) is not much modified by recycling, at least in the region of response-time limited performance where $\Delta P/\Delta I$ varies like ω^{-1}. The frequency response curve of a device is increased by recycling only below this cutoff but lines up with the response of a no-recycling system above this frequency. Hence, in spite of an apparent lower cutoff, there is no penalty in having some recycling at high speed. Next, let us discuss the possible compromise that arise between linewidth and bandwidth if speeds close to the gigabit per second rate are required: then, strong pumping of the diode structure is essential to reach high filling factors in the bands and reduce the spontaneous emission lifetime. This band filling has two effects: it brings the active layers closer to transparency and reduces correspondingly the recycling phenomenon. At the same time, it broadens the emitted spectrum, up to values as large as 0.2 eV if no special care is taken. This broad linewidth limits the benefit of microcavities by exceeding in many configurations the limit $S = S_{\rm esc}$. To optimize a device, it is critical in such cases that band engineering is carried out to produce a large speed (large filling factor, basically), without excessive broadening. This optimization is analogous to that made to optimize gain with minimal carrier density in laser structures (SCH, GRINSCH) and can be based on the wealth of models devised for existing structures. The coupling of such an electronic modeling of LED's with the present extraction modeling is probably required to attain the best linewidth/bandwidth compromise in these demanding conditions.

IV. Conclusion

By using an exact approach to the extraction cofficient of light from microcavity emitters, we could take into account the vector nature of light (dipole orientations and polarization effects) and Fresnel reflection coefficient as well as lifetime effects which depend on dipole orientation, etc. We calculated extraction per cycle for a typical emitter configuration with a metal mirror on one side and a DBR on the other side for any pair of indices $(n_{\mathrm{lo}}, n_{\mathrm{hi}})$, identified as a useful compromise in Part I [1]. The good agreement between both approaches at low index contrast Δn is made clear by comparing the maps of Fig. 3 in this paper with that of [1, Fig. 10]. This confirms that the effective cavity order m_c, taking into account DBR penetration, is the prominent factor determining monochromatic extraction as $\eta = 1/m_c$ in such microcavities. The studied asymmetric configuration is intended as a general starting point for further optimization. We optimized here the relative emitting wavelength λ/λ_B and the number of DBR pairs. We calculated how emitted power is shared among the various channels (outside, leaky, and guided modes, metal absorption). Spectral trends in this optimal case have been given from various points of view: evolution of monochromatic extraction with detuning, extraction from a Gaussian natural source, cavity extraction own's linewidth. As a general rule, spectral width S of the source tends to diminish the benefit of microcavity for extraction only beyond the material's intrinsic value S_{esc}, 4%–6% typically.

Using data from this configuration, the welcome effect of photon recycling was evaluated. It was shown that large extractions can be obtained in microcavity light emitters with much less demand on internal quantum efficiency. Trends for real systems at room temperature have been deduced, noting that requirement of spectral narrowing instead of overall extraction can lead to different conclusions depending on the application. Figures suggest that extraction of the order of 30%–50% can be realized in many systems, especially with the help of photon recycling. Thus, in all cases where LED's have the adequate frequency and spectral response, they appear at many wavelengths as possible contender's of vertical-cavity surface-emitting lasers (VCSEL's) in terms of efficiency, in particular in the low-cost end of the optoelectronic device spectrum, since requirements on a device based on spontaneous emission are as a rule far less stringent than those of devices based on stimulated emission (lasers and amplifiers). We thus foresee that a new generation of light emitters with semiconductors or other materials could stem from microcavity concepts.

Acknowledgment

The authors wish to thank particularly D. Labilloy, J. Blondelle, R. Houdré, and R. Stanley for their advice.

References

[1] H. Benisty, H. De Neve, and C. Weisbuch, "Impact of planar microcavity effects on light extraction—Part I: Basic concepts and analytical trends," this issue, pp. 1612–1631.

[2] G. B. Stringfellow and M. G. Craford, Eds., *High-Brightness Light-Emitting Diodes*. San Diego, CA: Academic, 1997.

[3] M. G. Craford, "Overview of device issues in high-brightness light-emitting diodes," in *High-Brightness Light-Emitting Diodes*, G. B. Stringfellow and M. G. Craford, Eds. San Diego, CA: Academic, 1997, pp. 47–64.

[4] W. Lukosz, "Theory of optical-environment-dependent spontaneous-emission rates for emitters in thin layers," *Phys. Rev. B*, vol. 22, pp. 3030–3038, 1980.

[5] ——, "Light emission by magnetic and electric dipoles close to a plane dielectric interface. III. Radiation patterns of dipoles with arbitrary orientation," *J. Opt. Soc. Amer.*, vol. 69, pp. 1495–1503, 1979.

[6] G. W. Ford and W. H. Weber, "Electromagnetic interaction of molecules with metal surfaces," *Phys. Rep.*, vol. 113, pp. 195–287, 1984.

[7] H. Benisty, M. Mayer, and R. Stanley, "A method of source terms for dipole emission modification in modes of arbitrary planar structures," *J. Opt. Soc. Amer. A*, vol. 15, pp. 1192–1201, 1998.

[8] H. De Neve, J. Blondelle, R. Baets, P. Demeester, P. Vandaele, and G. Borghs, "High efficiency planar microcavity LEDs: Comparison of design and experiments," *IEEE Photon. Technol. Lett.*, vol. 7, pp. 287–289, 1995.

[9] J. Blondelle, H. De Neve, P. Demeester, P. Vandaele, G. Borghs, and R. Baets, "16% external quantum efficiency from planar microcavity LED's at 940 nm by precise matching of cavity wavelength," *Electron. Lett.*, vol. 31, pp. 1286–1287, 1995.

[10] J. L. Bradshaw, R. P. Devaty, W. J. Choyke, and R. L. Messham, "Below-band-gap photon recycling in $Al_xGa_{1-x}As$," *Appl. Phys. Lett.*, vol. 55, pp. 165–167, 1989.

[11] T. Nishikawa, M. Yokota, S. Nakamura, Y. Kadoya, M. Yamanishi, and I. Ogura, "Influence of photon reabsorption on the transfer efficiency of output intensity in semiconductor microcavities," *IEEE Photon. Technol. Lett.*, vol. 9, pp. 179–181, 1997.

[12] T. Nishikawa, T. Kakimura, Y. Lee, and M. Yamanishi, "Enhanced transfer efficiency in AlGaAs asymmetric planar microcavities," *Appl. Phys. Lett.*, vol. 65, pp. 1796–1798, 1994.

[13] H. De Neve, J. Blondelle, P. Vandaele, P. Demeester, R. Baets, and G. Borghs, "Recycling of guided mode light emission in planar microcavity light emitting diodes," *Appl. Phys. Lett.*, vol. 70, pp. 799–801, 1997.

[14] I. Schnitzer, E. Yablonovitch, C. Caneau, and T. J. Gmitter, "Ultrahigh spontaneous emission quantum efficiency, 99.7% internally and 72% externally, from AlGaAs/GaAs/AlGaAs double heterostructures," *Appl. Phys. Lett.*, vol. 62, pp. 131–133, 1993.

[15] S. Adachi, "GaAs AlAs and GaAlAs: Material properties for use in research and device applications," *J. Appl. Phys.*, vol. 58, pp. R1–R29, 1985.

[16] L. A. Coldren and S. W. Scorzinne, *Diode Lasers and Photonic Integrated Circuits*. New York: Wiley, 1995.

[17] C. H. Henry, L. F. Johnson, R. A. Logan, and P. D. Clarke, "Determination of the refractive index of InGaAsP epitaxial layers by mode line luinescence spectroscopy," *IEEE J. Quantum Electron.*, vol. QE-21, pp. 1887–1892, 1985.

[18] T. L. Koch and U. Koren, "Photonic integrated circuits," in *Integrated Optoelectronics*, M. Dagenais, R. F. Leheny, and J. Crow, Eds. San Diego, CA: Academic, 1995, pp. 557–626.

[19] F. M. Steranka, "AlGaAs red light-emitting diodes in high-brightness light-emitting diodes, G. B. Stringfellow and M. G. Craford, Eds., *Semiconductors and Semimetals*. San Diego, CA: Academic, 1997 pp. 65–96.

[20] H. C. Casey and M. B. Panish, *Heterostructure Lasers, Vol. A and B*. New York: Academic, 1978.

[21] S. N. Mohammad, A. A. Salvador, and H. Morkoç, "Emerging gallium nitride base devices," *Proc. IEEE*, vol. 83, pp. 1305–1355, 1995.

[22] H. Morko, S. Strite, G. B. Gao, M. E. Lin, B. Sverldov, and M. Burns, "Large-band-gap SiC, III-V nitride and II-VI ZnSe-based semiconductor device technologies," *J. Appl. Phys.*, vol. 76, pp. 1363–1398, 1994.

[23] S. Nakamura, "III-V nitride based light-emitting devices," *Solid State Commun.*, vol. 102, pp. 237–248, 1997.

[24] ——, "Group III-V nitride-based ultraviolet blue-green-yellow light-emitting diodes and laser diodes," in *High-Brightness Light-Emitting Diodes*, G. B. Stringfellow and M. G. Craford, Eds. San Diego, CA: Academic, 1997, pp. 391–443.

[25] M. Koike, S. Yamasaki, S. Nagai, N. Koide, and S. Asami, "High-quality GaInN GaN multiple quantum wells," *Appl. Phys. Lett.*, vol. 68, pp. 1403–1405, 1996.

[26] M. A. Vidal, G. Ramirez-Flores, H. Navarro-Contreras, A. Lastras-Martinez, R. C. Powell, and J. E. Greene, "Refractive indices of zincblende structure β-GaN(001) in the subband-gap region (0.7–3.3 eV)," *Appl. Phys. Lett.*, vol. 68, pp. 441–443, 1996.

[27] F. A. Kish, F. M. Steranka, D. C. DeFevere, D. A. Vanderwater, K. G. Park, C. P. Kuo, T. D. Osentowski, M. J. Peanasky, J. G. Yu, R.

M. Fletcher, D. A. Steigerwald, M. G. Craford, and V. M. Robbins, "Very-high efficiency semiconductor wafer-bonded transparent-substrate $(Al_xGa_{1-x})_{0.5}In_{0.5}P$/GaP light-emitting diodes," *Appl. Phys. Lett.*, vol. 64, pp. 2839–2841, 1994.
[28] F. A. Kish and R. M. Fletcher, "AlGaInP light-emitting diodes," in *High-Brightness Light-Emitting Diodes*, G. B. Stringfellow and M. G. Craford, Eds. San Diego, CA: Academic, 1997, pp. 149–226.
[29] G. E. Höfler, D. A. Vanderwater, D. C. DeFevere, F. A. Kish, M. D. Camras, F. M. Steranka, and I. H. Tan, "Wafer bonding of 50-mm diameter GaP to AlGaInP-GaP light-emitting diode wafers," *Appl. Phys. Lett.*, vol. 69, pp. 803–805, 1996.
[30] A. Salokatve, A. Salokatve, K. Rakennus, P. Uusimaa, M. Pessa, T. Aherne, J. P. Doran, J. O'Gorman, and J. Hegarty, "Growth and characterization of an epitaxially grown ZnSSe/MnZnSSe distributed Bragg reflector," *Appl. Phys. Lett.*, vol. 67, pp. 407–409, 1995.
[31] Y.-H. Wu, "Structure-dependent threshold current density for CdZnSe-based II-VI semiconductor lasers," *IEEE J. Quantum Electron.*, vol. 30, pp. 1562–1573, 1994.
[32] C. Brys, F. Vermaerke, P. Demeester, P. V. Daele, K. Rakennus, A. Salokatve, P. Uusimaa, M. Pessa, A. L. Bradley, J. P. Doran, J. O'Gorman, and J. Hegarty, "Epitaxial lift-off of ZnSe based II-VI structures," *Appl. Phys. Lett.*, vol. 66, pp. 1086–1088, 1995.
[33] A. Tsujimura, S. Yoshi, S. Hayashi, K. Ohkawa, and T. Mitsuyu, "Cavity parameters of ZnCdSe/ZnSe single-quantum-well separate-confinement-heterostructure laser diodes," *Jpn. J. Appl. Phys.*, vol. 32, pp. L1750–L1752, 1993.
[34] D. G. Deppe and C. Lei, "Spontaneous emission from a dipole in a semiconductor microcavity," *J. Appl. Phys.*, vol. 70, pp. 3443–3448, 1991.
[35] G. Björk, S. Machida, Y. Yamamoto, and K. Igeta, "Modification of spontaneous emission rate in planar dielectric microcavity structures," *Phys. Rev. A*, vol. 44, pp. 669–681, 1991.
[36] N. E. J. Hunt, N. E. J. Hunt, E. F. Schubert, D. L. Sivco, A. Y. Cho, R. F. Kopf, R. A. Logan, and G. J. Zydzik, "High efficiency, narrow spectrum resonant-cavity light-emitting diodes," in *Confined Electrons and Photons*, E. Burstein and C. Weisbuch, Eds. New York: Plenum, 1995, pp. 703–714.
[37] R. R. Chance, A. Prock, and R. Silbey, "Fluorescence and energy transfer near interfaces," in *Advances in Chemical Physics*, I. Prigogine and S.A. Rice, Eds. New York: Wiley, 1978, pp. 1–65.
[38] M. G. Craford, "Commercial light emitting diode technology: Status, trends and possible future performances," in *Microcavities and Photonic Bandgaps: Physics and Application*, J. Rarity and C. Weisbuch, Eds. Dordrecht, The Netherlands: Kluwer, NATO ASI Series, 1996, pp. 323–332.
[39] S. T. Ho, D. Y. Chu, J.-P. Zhang, S. Wu, and M. Chin, "Dielectric photonic wells and wires and spontaneous coupling efficiency of microdisk and photonic-wire semiconductor lasers in optical processes in microcavities," R. K. Chang and A. J. Campillo, Eds., *Advanced Series in Applied Physics*. Singapore: World Scientific, 1996, pp. 339–388.
[40] P. Wittke, "Spontaneous emission rate alteration by dielectric and other waveguiding structures," *RCA Rev.*, vol. 36, pp. 655–660, 1975.
[41] S. T. Ho, S. L. Mc Call, and R. E. Slusher, "Spontaneous emission from excitons in thin dielectric layers," *Opt. Lett.*, vol. 18, pp. 909–911, 1993.
[42] J. Blondelle, H. De Neve, P. Demeester, P. Vandaele, G. Borghs, and R. Baets, "6-percent external quantum efficiency from InGaAs/(Al)GaAs single-quantum-well planar microcavity LED's," *Electron. Lett.*, vol. 30, pp. 1787–1788, 1994.
[43] J. Blondelle, H. De Neve, G. Borghs, P. Vandaele, P. Demeester, and R. Baets, "High efficiency $(>20\%)$ microcavity LED's," in *IEE Colloquium on Semiconductor Optical Microcavity Devices and Photonic Bandgaps*, London, U.K., 1996.
[44] J. Blondelle, "Realization of high-efficiency substrate-emitting InGaAs/(Al)GaAs microcavity LED's by means of MOCVD," Ph.D. dissertation, University of Gent, Belgium, 1997.
[45] H. De Neve, J. Blondelle, P. Vandaele, P. Demeester, R. Baets, and G. Borghs, "Planar substrate-emitting microcavity light emitting diodes with 20% external QE," presented at SPIE Photonics West, San Jose, CA, 1997.
[46] H. De Neve, "Study and realization of microcavity based LED's," Ph.D. dissertation, University of Gent, Belgium, 1997.
[47] A. Kastler, "Atomes à l'intérieur d'un interféromètre Perot-Fabry," *Appl. Opt.*, vol. 1, pp. 17–24, 1962.
[48] E. U. Condon and H. Odishaw, Eds., *American Institute of Physics Handbook*. New York: McGraw-Hill, 1967.
[49] R. L. Moon, "MOVPE: Is there any technology for optoelectronics?," *J. Cryst. Growth*, vol. 170, pp. 1–10, 1997.
[50] J. Bleuse, E. Hadji, N. Magnea, and J.-L. Pautrat, "II-VI resonant cavity light emitting diodes for the mid-infrared," in *Microcavities and Photonic Bandgaps*, J. Rarity and C. Weisbuch, Eds. Dordrecht, The Netherlands: Kluwer, NATO ASI Series, 1996, pp. 353–362.
[51] G. Bastard, *Wave Mechanics Applied to Semiconductor Heterostructures*. Les Ulis, France: Les Editions de Physique, 1990.
[52] N. E. J. Hunt, A. M. Vredenberg, E. F. Schubert, E. F. Becker, D. C. Jacobson, J. M. Poate, and G. J. Zydzik, "Spontaneous emission control in planar structures: Er3+ in Si/SiO2 microcavities," in *Confined Electrons and Photons*, E. Burstein and C. Weisbuch, Eds. New York: Plenum Press, 1995, pp. 703–714.
[53] N. E. J. Hunt, E. F. Schubert, R. A. Logan, and G. J. Zydzik, "Enhanced spectral power density and reduced linewidth at 1.3 μm in an InGaAsP quantum well resonant cavity light-emitting diode," *Appl. Phys. Lett.*, vol. 61, pp. 2287–2289, 1992.
[54] K. Neyts, "Cavity effects in thin film phosphors based on ZnS," in *Microcavities and Photonic Bandgaps: Physics and Applications*, J. Rarity and C. Weisbuch, Eds. Dordrecht, The Netherlands: Kluwer, NATO ASI Series, 1996, pp. 397–406.
[55] E. F. Schubert, N. E. J. Hunt, R. J. Malik, M. Micovic, and D. L. Miller, "Temperature and Modulation characteristics of resonant-cavity light-emitting diodes," *J. Lightwave Technol.*, vol. 14, pp. 1721–1728, 1996.

H. Benisty, photograph and biography not available at the time of publication.

H. De Neve, photograph and biography not available at the time of publication.

C. Weisbuch, photograph and biography not available at the time of publication.